SCIENTIFIC REPORTS

OPEN

Chemical synthesis of hierarchical $NiCo_2S_4$ nanosheets like nanostructure on flexible foil for a high performance supercapacitor

Received: 26 May 2017
Accepted: 26 July 2017

D. -Y. Kim[1], G. S. Ghodake[1], N. C. Maile[2], A. A. Kadam[3], Dae Sung Lee[4], V. J. Fulari[2] & S. K. Shinde[1]

In this study, hierarchical interconnected nickel cobalt sulfide ($NiCo_2S_4$) nanosheets were effectively deposited on a flexible stainless steel foil by the chemical bath deposition method (CBD) for high-performance supercapacitor applications. The resulting $NiCo_2S_4$ sample was characterized by X-ray powder diffraction (XRD), field emission scanning electron microscopy (FE-SEM), high-resolution transmission electron microscopy (HR-TEM), and electrochemical measurements. XRD and X-ray photoelectron spectroscopy (XPS) results confirmed the formation of the ternary $NiCo_2S_4$ sample with a pure cubic phase. FE-SEM and HR-TEM revealed that the entire foil surface was fully covered with the interconnected nanosheets like surface morphology. The $NiCo_2S_4$ nanosheets demonstrated impressive electrochemical characteristics with a specific capacitance of 1155 $F\,g^{-1}$ at 10 $mV\,s^{-1}$ and superior cycling stability (95% capacity after 2000 cycles). These electrochemical characteristics could be attributed to the higher active area and higher conductivity of the sample. The results demonstrated that the interconnected $NiCo_2S_4$ nanosheets are promising as electrodes for supercapacitor and energy storage applications.

In recent years, supercapacitor/energy storage devices have emerged as devices with great potential because of the rapid expansion of new and environmentally friendly energy conversion and storage devices[1–7]. Supercapacitors, which are useful energy storage devices for hybrid electric vehicles, and batteries, have attracted considerable attention because of their high power density and long-life cycling stability that are comparable to other batteries[4, 8–11]. The capabilities of supercapacitors mostly depend on the active electrode materials, and they can generally be divided into three main types: transition metal oxides, carbon materials, and conducting polymers[4].

Various transition metal oxides are used in supercapacitors, such as RuO_2[12], NiO[13], ZnO/NiO[14], CuO[15], $NiCoO_2$[16], CuO[17], CoO[18, 19], FeO_2[20], and MnO_2[21], and metal sulfides such as NiS[22], MnS[23, 24], CoS[25], CoS_2[26], and $CuCo_2O_4$;[27] these are attractive electrode materials for supercapacitor applications. Recently, transition metal chalcogenides are increasingly used in supercapacitor applications. Sulfur ions tend to produce flexible nanostructures because of higher electroconductive properties and fast charge transportation[28]. In comparison with binary and ternary metal oxides, ternary metal sulfides are more popular because of the higher levels active redox species, fast charge-discharge, and long-time stability. Among them, nickel cobalt sulfide ($NiCo_2S_4$) has attracted significant interest because of its environmentally stable nature, high redox reactions[29], high theoretical specific capacitance, and high electronic conductivity[30].

To date, thin films of ternary $NiCo_2S_4$ have been widely studied by various researchers. The films have been deposited using various techniques such as the calcination[31], hydrothermal[32] via a gas bubble soft template and

[1]Department of Biological and Environmental Science, College of Life Science and Biotechnology, Dongguk University-Seoul, Biomedical Campus-Ilsan, Goyang-si, Gyeonggi-do, 10326, South Korea. [2]Holography and Materials Research Laboratory, Department of Physics, Shivaji University, Kolhapur, 416 004, Maharashtra, India. [3]Research Institute of Biotechnology and Medical Converged Science, Dongguk University, Biomedi Campus, Ilsandong-gu, Goyang-si, Gyeonggi-do, 10326, Republic of Korea. [4]Department of Environmental Engineering, Kyungpook National University, 80 Daehak-ro, Buk-Gu, Daegu, 41566, Republic of Korea. Correspondence and requests for materials should be addressed to S.K.S. (email: surendrashinde.phy@gmail.com)

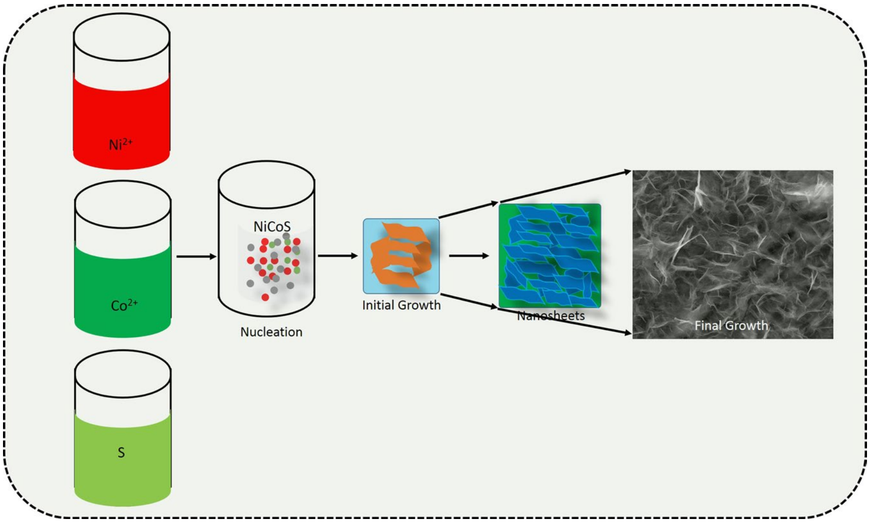

Figure 1. Schematic illustration of the preparation process of the nanosheets like $NiCo_2S_4$ thin films.

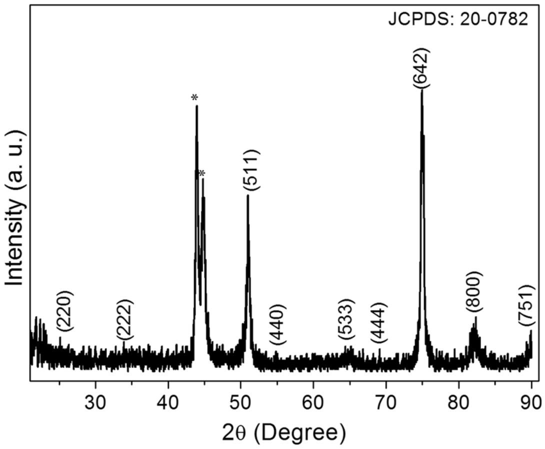

Figure 2. XRD pattern for the $NiCo_2S_4$ sample on the flexible stainless steel foil.

hydrothermal[33], the sputtering[34], and the sulfur-bubble template methods[35]. Among the various available methods, the chemical bath deposition method is one of the simple, cheap, and attractive method.

Yu *et al.*[36]. have prepared $NiCo_2S_4$ using the hydrothermal method. They reported that the capacitance was 720 mAh g^{-1} after 50 cycles, which was similar to the theoretical capacity of $NiCo_2S_4$ electrodes. Jia *et al*[37]. have synthesized $NiCo_2S_4$ electrodes and $NiCo_2S_4@Fe_2O_3$ on Ti substrates using a simple electrodeposition method for asymmetric supercapacitor application. The research group developed an asymmetric supercapacitor with the $NiCo_2S_4/Fe_2O_3$ electrode. The specific capacitance of the asymmetric cell was determined as 342 F g^{-1} at a scan rate of 5 mV s^{-1}. In another study, Li *et al*[38]. described a facile and commendable method to produce hierarchical $NiCo_2S_4/Co(OH)_2$ nanotubes on Ni foam. They reported that $NiCo_2S_4/Co(OH)_2$ electrodes have a high area capacitance compared with $NiCo_2S_4$ electrodes. Zhu *et al*[39]. have prepared $NiCo_2S_4$ thin films via the solvothermal route for supercapacitor applications. They developed $NiCo_2S_4$ nanoparticles with an ultrahigh specific capacitance of 1440 F g^{-1} at 3 A g^{-1} after 250 cycles. Su *et al*[40]. have synthesized $NiCo_2S_4$ electrodes using the solvothermal method for dye-sensitized solar cell (DSC) application, demonstrated the maximum cell efficiency of 8.94% on an ITO-coated glass substrate.

By using a facile chemical bath deposition method in this study, we effectively synthesized interconnected $NiCo_2S_4$ nanosheets on a flexible stainless steel foil for high-performance supercapacitor applications. The specific capacitance of the as-synthesized $NiCo_2S_4$ nanosheets revealed good cycling stability and a long charging-discharging time. Our results indicated that the interconnected $NiCo_2S_4$ nanosheets can be used as high-performance materials for supercapacitor applications.

Experimental Section

Materials. 0.1 M nickel (II) sulfate ($NiSO_4(H_2O)_6$), 0.2 M cobalt (II) sulfate ($CoSO_4{\cdot}7H_2O$), and 0.2 M sodium sulfide ($Na_2S\ 6H_2O$) were dissolved in 20 mL of deionized water with ammonia (NH_3).

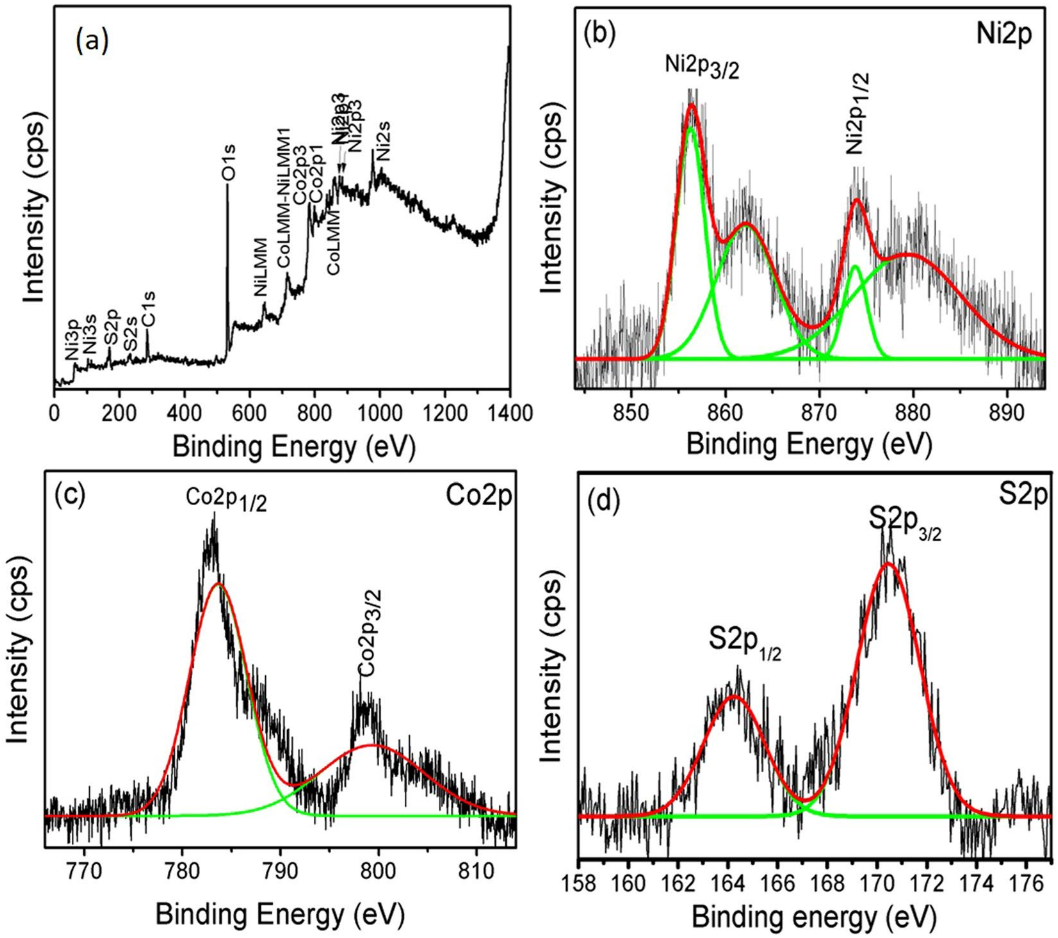

Figure 3. (**a**) XPS survey spectrum of $NiCo_2S_4$ sample, (**b**) high resolution spectrum of Ni2p, (**c**) high resolution spectrum of Co2p, (**d**) high resolution spectrum of S2p.

Synthesis and growth mechanism of $NiCo_2S_4$. The proposed growth mechanism of the chemical bath deposited $NiCo_2S_4$ nanosheet-like nanostructured thin films is explained using following steps. Initially, to generate Ni^{2+} and Co^{2+}, the nickel(II) sulfate ($NiSO_4(HO)_6$) and cobalt(II) sulfate ($CoSO_4{\cdot}7H_2O$) were dissolved in the double-distilled water, sodium sulfide ($Na_2S{\cdot}6H_2O$) was used as the precipitant for S^{2-} ions, and ammonia was used as a complexing agent for adjusting the pH to 11. Then, a well cleaned flexible stainless steel foil was immersed in the prepared bath and maintained at room temperature. During precipitation, nickel cobalt sulfide was deposited on the foil. After 2 h, the flexible nickel cobalt sulfide thin films deposited on the stainless steel foil was removed from the solution bath, washed with double-distilled water, dried in ambient air, and preserved in an airtight container. Deposition time is associated with nucleation ratio and growth activities. The attached nanoparticle developed along a specific crystal orientation according to the attachment and arrangement of the 3D nanostructure as shown in Fig. 1. The developmental steps of the 3D interconnected nanosheets of nickel cobalt sulfide were as follows: nucleation, growth, and oriented attachment of the nanomaterial. Nucleation is related to the total volume of the supersaturation ions in the solution. In the nucleation stage, supersaturation is extremely high, and electrostatic repulsive barriers are low; hence, particles tend to aggregate[41].

Characterization. The structures and morphology of $NiCo_2S_4$ thin films were characterized by X-ray powder diffraction (XRD; CuK_α radiation, $\lambda = 0.154$ nm), X-ray photoelectron spectroscopy (XPS; ULVAC-PHI Quantera SXM), field emission scanning electron microscopy (FE-SEM; QUANTA 400 F), and high resolution transmission electron microscopy, (TEM; Titan G2 ChemiSTEM Cs Probe) with an energy-dispersive X-ray spectroscopy (EDS) detector.

Electrochemical performance test. The area of $NiCo_2S_4$ on the flexible stainless steel foil deeped into the electrolyte was kept constant. Electrochemical tests were conducted with a CHI 660E electrochemical workstation in aqueous 1 M KOH electrolyte using a three-electrode cell where the platinum electrode served as the counter electrode, the $NiCo_2S_4$ electrode served as the working electrode, and a standard calomel electrode (SCE) served as the reference electrode.

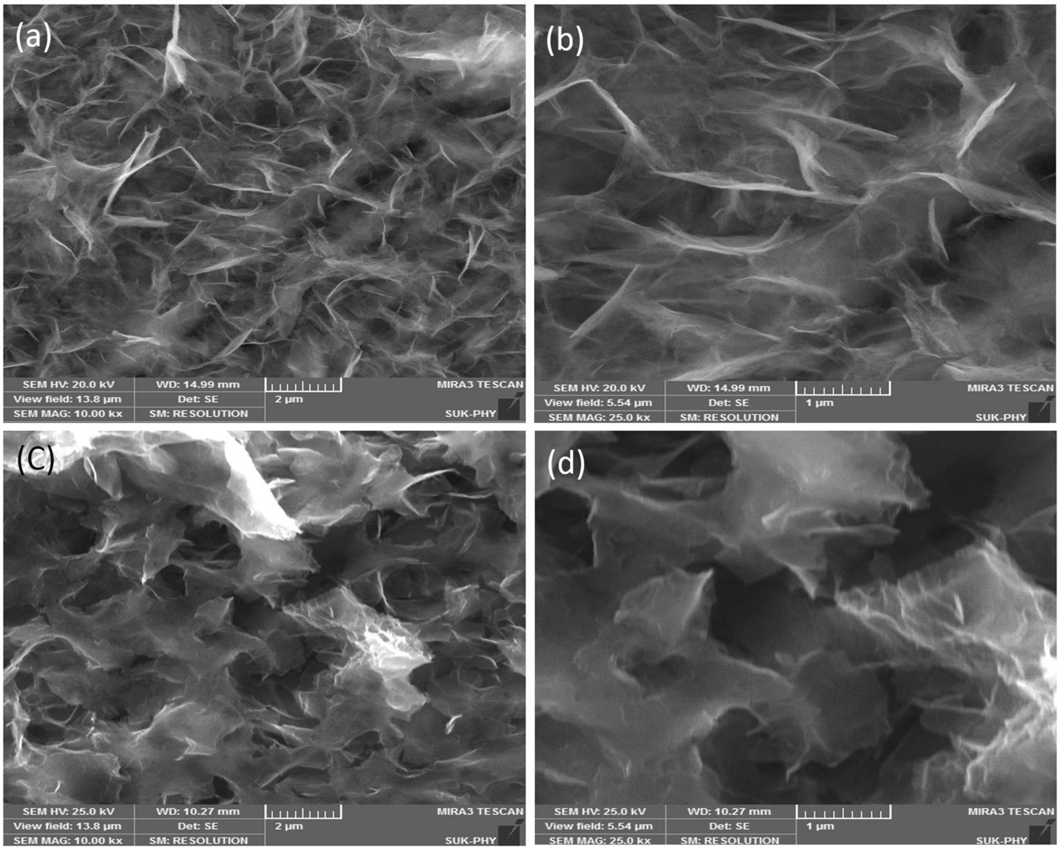

Figure 4. (**a**,**b**) FE-SEM images of $NiCo_2S_4$ sample prepared by chemical bath deposition method, and (**c**,**d**) FE-SEM images of $NiCo_2S_4$ sample after stability testing with different magnifications.

Results and Discussion

To identify and determine the phase of the $NiCo_2S_4$ sample prepared by the chemical bath deposition method, we first performed XRD measurements, as shown in Fig. 2. Figure 2 shows the XRD pattern of the $NiCo_2S_4$ sample on the flexible stainless steel foil. The diffraction peaks positioned at 25.14°, 33.84°, 51.03°, 54.95°, 66.24°, 69.17°, 74.90°, 82.44°, and 90.74° were indexed to the (220), (222), (511), (440), (533), (444), (642), (800), and (751) planes of the cubic phase of the $NiCo_2S_4$ sample, and all peaks were well matched with the data of the Joint Committee on Powder Diffraction Standards (JCPDS 20-0782). The strong peaks at 43.93° and 44.77° corresponded to the flexible stainless steel foil. The most intense peak was located at 74.90°,suggesting the pure/single phase of the $NiCo_2S_4$ material. No other phases such as NiO, CoO, $NiCoO_4$, NiS, and CoS were observed in the $NiCo_2S_4$ sample. This result is in agreement with that of a previous study on $NiCo_2S_4$ synthesized by a different method[42–44]. XRD results demonstrated that the chemical bath deposition method is suitable for the preparation of single-phase nanomaterials for applications in energy storage devices. In addition, XRD results are consistent with the results of XPS and FE-SEM.

The chemical state and elemental composition of $NiCo_2S_4$ nanosheets were investigated by XPS measurements, and the corresponding results are shown in Fig. 3(a–d). Figure 3a shows a XPS spectrum of $NiCo_2S_4$ in which peaks are located at 783.24 eV and 798.02 eV corresponded to Co2p, 856.52 eV and 874.03 eV corresponded to Ni2p, and 164.28 eV and 170.57 eV corresponded to S2p, indicating the presence of Ni, Co, and S elements in the $NiCo_2S_4$ sample[45, 46]. In addition, C and O elements were present. The O element was observed because the sample was prepared in double-distilled water. Figure 3(b–d) shows that the high-resolution spectra of the Ni2p, Co2p, and S2p elements can be fitted using a Gaussian fitting method. As shown in Figure S1b, the intensity of all the presented peaks was higher than O1s. Figure 3b shows the high-resolution spectrum of Ni2p. Based on Fig. 3b, the binding energies of 856.52 eV and 874.03 eV were associated with Ni^{2+},whereas those of 862.69 eV and 880.96 eV were associated with Ni^{3+} [42]. Figure 3c shows the high-resolution spectrum of the Co2p energy level. The binding energies of 783.24 eV and 798.03 eV indicated Co2p, which confirmed that the Co element was present in the $NiCo_2S_4$ sample[42]. Similarly, Fig. 3d shows the high-resolution spectrum of the S2p peak. The binding energies of 164.28 eV and 170.57 eV corresponded to the $S2p_{1/2}$ and $S2p_{3/2}$ energy state of S2p. Figure S1 (a, b) shows the core level of the C1s and O1s elements of the $NiCo_2S_4$ sample[42, 45–48]. These XPS results are comparable with previous XRD analysis results.

FE-SEM was carried out to obtain further surface information and determine the porosity of the prepared $NiCo_2S_4$ samples before and after stability testing (2000 cycles). Figure 4 (a–d) displays the FE-SEM image of the $NiCo_2S_4$ thin films prepared by the chemical bath deposition method before and after testing the stability of

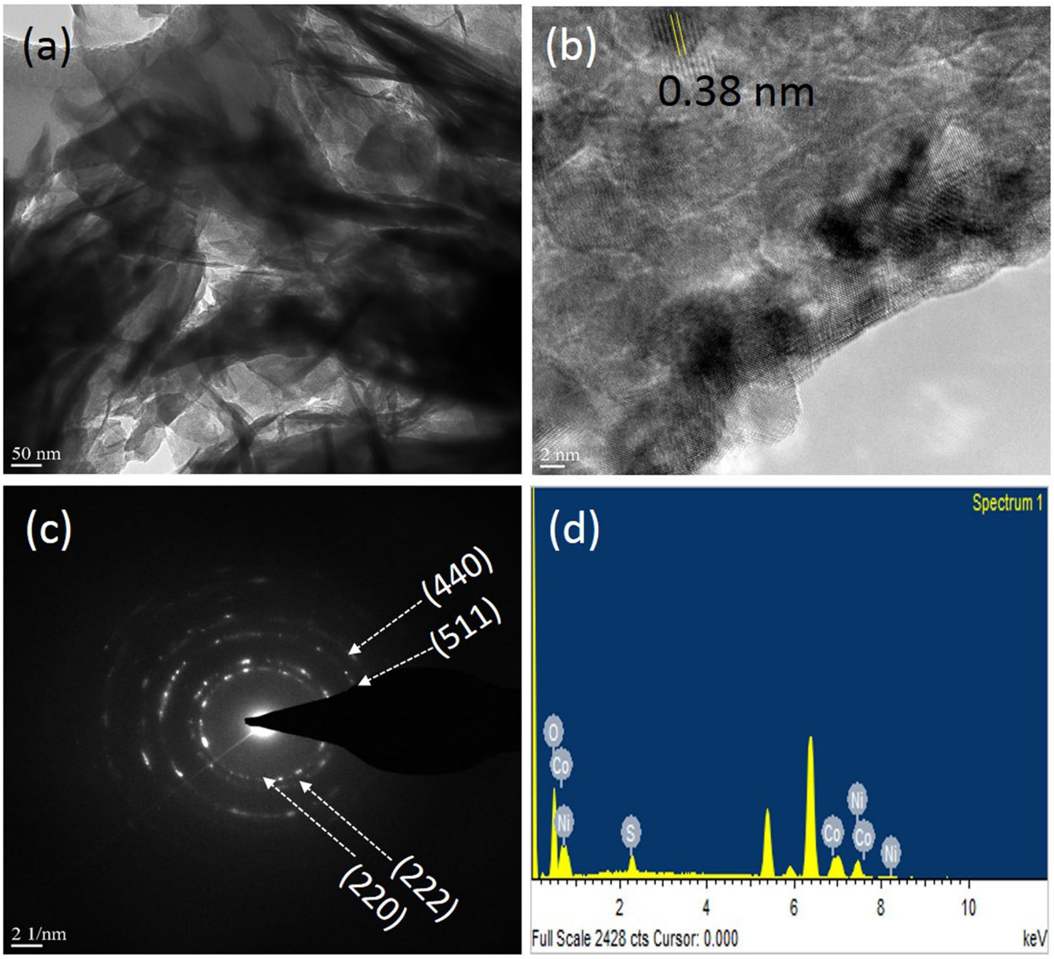

Figure 5. HR-TEM images (**a**,**b**), SAED pattern (**c**), and EDS (**d**), of $NiCo_2S_4$ sample.

the $NiCo_2S_4$ electrode. Figure 4 (a,b) clearly shows the 3D architecture with the interconnected, highly porous grapheme sheets-like nanosheets distributed on the flexible stainless steel foil[49]. The interconnected uniform 3D nanosheet-like nanostructures of $NiCo_2S_4$ had a thickness of ~30–40 nm. The nanosheets were highly flexible, transparent, and interconnected to each other and had a very low thickness, which demonstrated the large specific surface area of $NiCo_2S_4$[50]. Figure 4(c,d) shows the FE-SEM image of the $NiCo_2S_4$ sample after stability testing. A comparison between Fig. 4(a,b) and Fig. 4(c,d) revealed no change in surface morphology after testing the stability of the sample, thus indicating that the $NiCo_2S_4$ sample is stable. Based on electrochemical measurements, these nanostructures would be beneficial for ion diffusion.

High-resolution transmission electron microscopy (HR-TEM) was used to perform a detailed assessment of the surface morphology and structural foundation of the $NiCo_2S_4$ sample for supercapacitor applications. Figure 5(a,b) displays typical TEM images of the $NiCo_2S_4$ graphene nanosheets. Figure 5a clearly shows that the length of $NiCo_2S_4$ graphene nanosheets was approximately 90–110 nm, and the graphene nanosheet thickness was approximately 7–10 nm, which indicated the capability for high performance. The interconnected nanosheets result in a larger reactive surface area for supercapacitor applications. Selected area electron diffraction (SAED) pattern was obtained from the HR-TEM image of the $NiCo_2S_4$ sample shown in Fig. 5c. We measured the lattice spacing of the $NiCo_2S_4$ sample in Fig. 5b. The measured lattice spacing was 0.38 nm, which was correlated to the (440) plane of the cubic phase. The graphene-like nanosheets of $NiCo_2S_4$ uniformly covered the flexible stainless steel foil as shown in Fig. 5(a,b), thus supporting the results of FE-SEM. In addition, EDS analysis was conducted to study the elemental composition of Ni, Co, and S. Figure 5d shows the EDS results of the $NiCo_2S_4$ sample, which indicated the presence of the Ni, Co, and S elements in $NiCo_2S_4$. The results are in agreement with those of XPS. Figure 6 shows the EDS mapping of the $NiCo_2S_4$ sample, which revealed that the Ni, Co, and S elements were equally distributed in the sheets.

To determine its potential as a candidate for supercapacitor applications, we evaluated the electrochemical performance of the $NiCo_2S_4$ electrode on the flexible stainless steel foil in 1 M KOH electrolyte. Figure 7a displays the typical cyclic voltammetry (CV) curves of the $NiCo_2S_4$ electrode on the flexible stainless steel foil with a potential window of between −0.1 and 0.6 V (Vs SCE) at different scan rates (10–100 $mV\,s^{-1}$). In the cyclic voltammogram, there was a distinct pair of reduction and oxidation peaks at 0.1 V, 0.35 V, and 0.40 V, which may

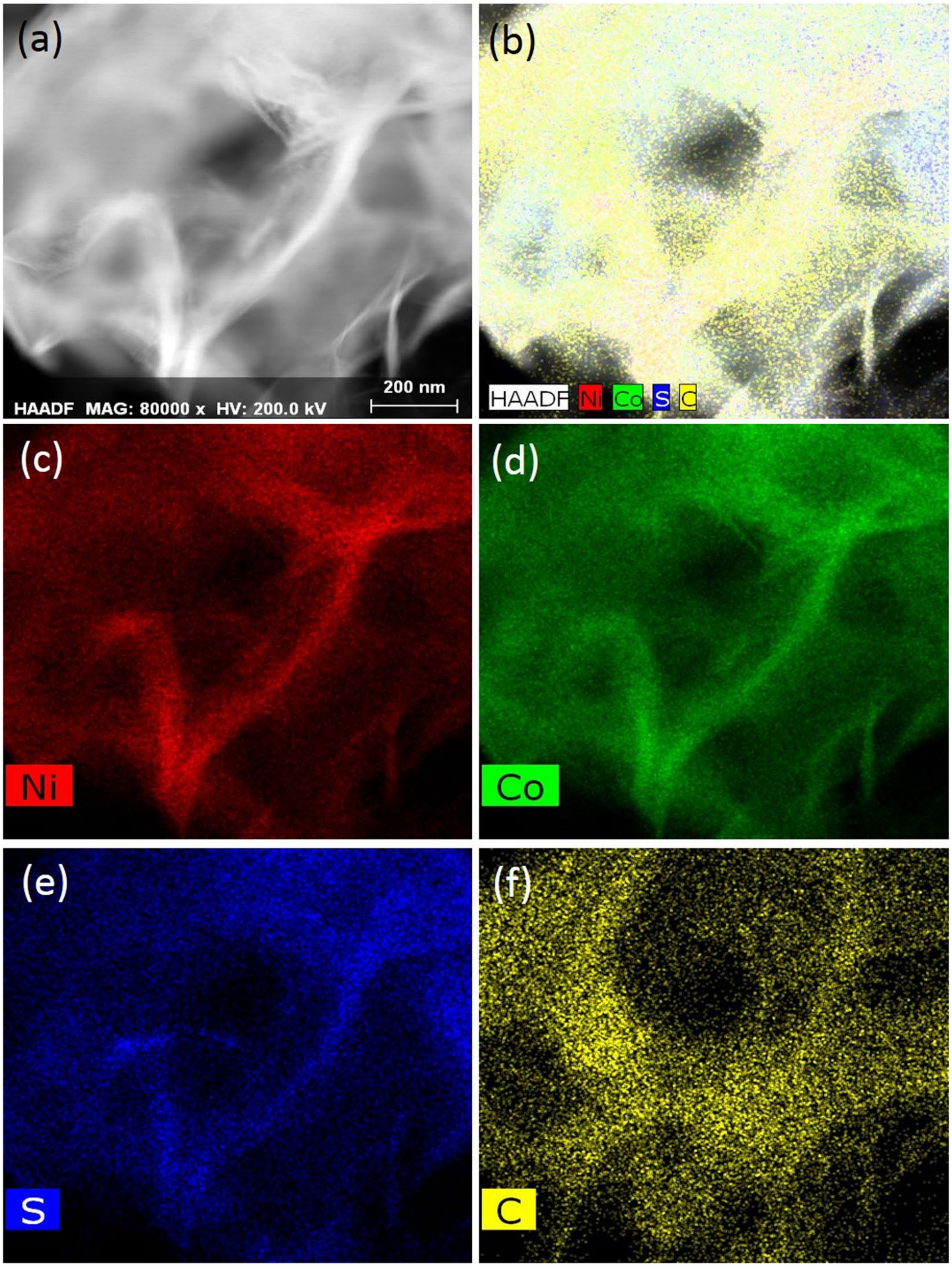

Figure 6. EDS mapping of the $NiCo_2S_4$ sample prepared by chemical bath deposition method.

be attributed to the redox reactions of the $NiCo_2S_4$ electrode in KOH electrolyte[51, 52]. CV demonstrated that the scan rate was increased, and the cathodic current and anodic current densities were increased according to the scan rate (10–100 mV s^{-1}), thus indicating the lower resistance of the $NiCo_2S_4$ electrode and fast redox reactions during the electrochemical process. Figure 7b shows the specific capacitance of the $NiCo_2S_4$ electrode at 10–100 mVs^{-1} scan rates in 1 M KOH. A high specific capacitance of 1155 Fg^{-1} was achieved at a scan rate of 10 mV s^{-1}, which is comparatively higher than that previously reported in other studies. Zhao *et al*[53]. have prepared $CoNi_2S_4$ thin films using the hydrothermal method for supercapacitor applications and obtained a maximum specific capacitance of 231.1 mAh g^{-1} at 2 A g^{-1}. Pu *et al*[48]. have synthesized $NiCo_2S_4$ hexagonal nanoplates with a specific capacitance of 437 F g^{-1} at a current rate of 1 A g^{-1} in 3 M KOH aqueous electrolyte.

Figure 7c shows the charge-discharge curves of the $NiCo_2S_4$ electrode at 1–5 $mAcm^{-1}$ current densities. Based on the charge-discharge curves of the $NiCo_2S_4$ electrode, we found that the mirror image of the sample

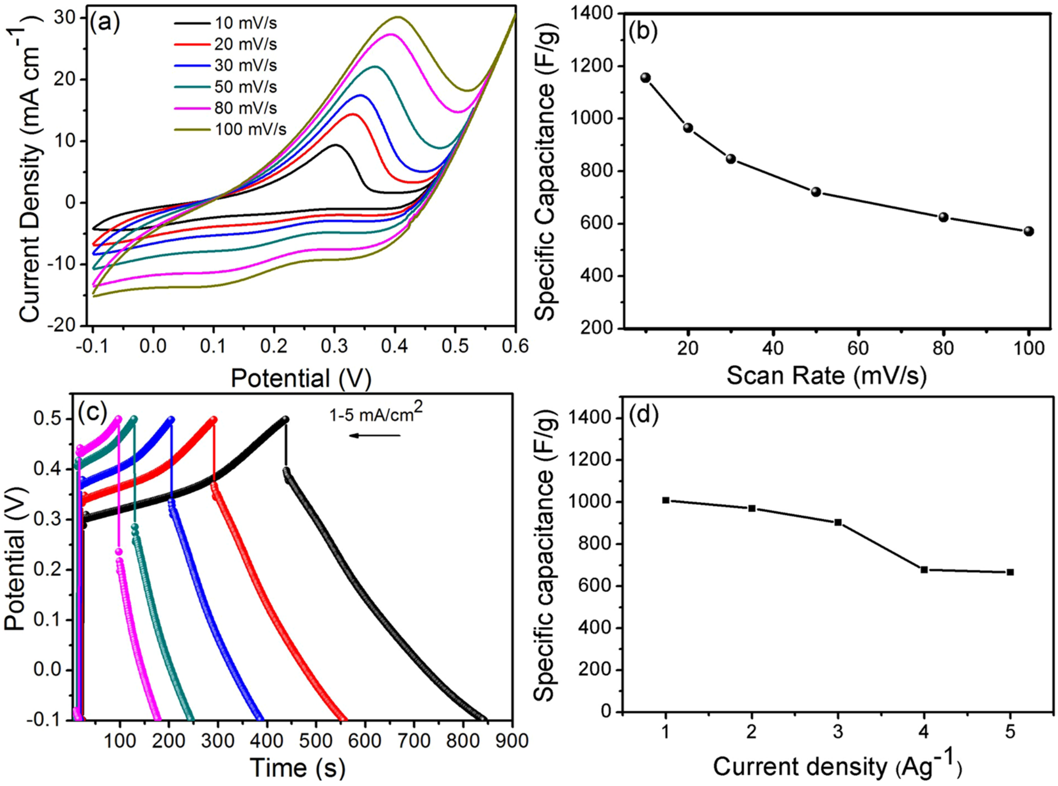

Figure 7. Cyclic voltammetry (CV) curves at different scan rates (**a**), specific capacitance as a function of scan rate (**b**), charging/discharging curves at different current density (**c**), specific capacitance as a function of different current density (**d**), of $NiCo_2S_4$ sample prepared by chemical bath deposition method.

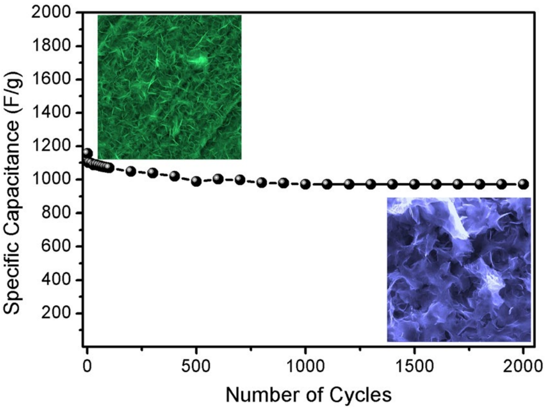

Figure 8. Cycling performance of the $NiCo_2S_4$ electrode at constant scan rate of 100 mV/s.

corresponded to the redox reactions during the electrochemical process. In addition, we observed that as the current density increased, the discharge time decreased. The specific capacitances were calculated based on these charge-discharge curves using the following equation:

$$C = \frac{I \times \Delta t}{m \times \Delta V} \quad (1)$$

where, C (F g^{-1}) is the specific capacitance of the electrode, I (A) is the current, Δt (s) is the discharge time, ΔV (V) is the potential window, and m (g) is the mass of active $NiCo_2S_4$ materials. Figure 7d shows the specific capacitance of the $NiCo_2S_4$ electrode with different current densities. Figure 7b and Fig. 7d show similar values of the specific capacitance of the as-synthesized $NiCo_2S_4$ sample. The maximum specific capacitance of the $NiCo_2S_4$ electrode was 1009 F g^{-1} at a current density of 1 mAcm^{-1}. The graph shows that as the current densities were

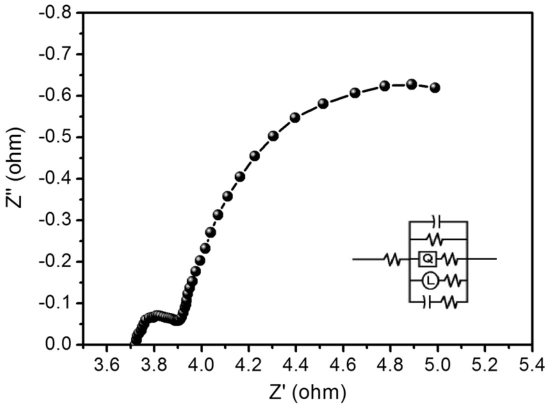

Figure 9. Nyquist plot of $NiCo_2S_4$ sample.

increased, the corresponding specific capacitances were decreased. The calculated specific capacitance was higher than that previously reported in the literature[54–56].

The most important feature in a supercapacitor is the stability of the materials. To determine the stability of the $NiCo_2S_4$ electrode, the values of specific capacitance with respect to the number of CV cycles at a scan rate of 100 mV s^{-1} were measured[48], as shown in Figure S2. Figure 8 shows the cycling stability of the $NiCo_2S_4$ electrodes. Figure 8 shows that after the cycling stability testing of the $NiCo_2S_4$ electrodes for 2000 cycles, the specific capacitance was decreased from 1155 to 995 F g^{-1} with a retention of 95%, which was improved in the previously reported $NiCo_2S_4$ samples[48, 56]. This result suggests that the $NiCo_2S_4$ electrode surface is stable during electrochemical reactions; thus, it can be used as a potential material for supercapacitor application.

To further understand the mechanism of charge transport and ion diffusion of the $NiCo_2S_4$ electrodes, we performed electrochemical impedance spectroscopy (EIS). EIS measurements were carried out in a frequency range from 100 kHz to 0.01 Hz. Figure 9 shows the Nyquist plots of the $NiCo_2S_4$ electrode synthesized by the chemical bath deposition method. As shown in Fig. 9, semicircles were observed in the high-frequency region, which may be attributed to the resistance of the KOH electrolyte[57]. The linear part of semicircles shows the inclement of the ion diffusion process. The slopes of around 45° in the Nyquist plot indicated the fast ion transfer between the electrode and electrolyte. The values of solution resistance (R_s) 3.6 Ω and charge transfer resistance (R_{ct}) 0.2 Ω are very small. Charge transfer resistance values were low, suggesting that the $NiCo_2S_4$ electrode is suitable for supercapacitor and energy storage applications.

Conclusion

In this study, novel hierarchical interconnected $NiCo_2S_4$ nanosheets were synthesized on a flexible stainless steel foil using the chemical bath deposition method for high-performance supercapacitors. The nanosheet-like nanostructures of the $NiCo_2S_4$ electrode had a high surface area, specific capacitance of 1155 F g^{-1} at a scan rate 10 mV s^{-1}, low solution resistance (3.4 Ω), low charge transfer resistance (0.2 Ω), and good cycling stability after 2000 cycles at 100 mV s^{-1}. We proposed that the synthesized $NiCo_2S_4$ nanosheets are promising as electrodes for high-performance energy storage devices.

References

1. Miller, J. R. & Simon, P. Electrochemical capacitors for energy management. *Science* **321**, 651, doi:10.1126/science.1158736 (2008).
2. Simon, P. & Gogotsi, Y. Materials for electrochemical capacitors. *Nat. Mater.* **7**, 845, doi:10.1038/nmat2297 (2008).
3. Hadjipaschalis, I., Poullikkas, A. & Efthimiou, V. Overview of current and future energy storage technologies for electric power applications. *Renew. Sustain. Energy Rev.* **13**, 1513, doi:10.1016/j.rser.2008.09.028 (2009).
4. Zhu, Y. *et al.* Mesoporous $NiCo_2S_4$ nanoparticles as high-performance electrode materials for supercapacitors. *J. Power Sources* **273**, 584, doi:10.1016/j.jpowsour.2014.09.144 (2015).
5. Pang, H. *et al.* synthesis of heterogeneous Co_3O_4-nanocube/$Co(OH)_2$-nanosheet hybrids for high-performance flexible asymmetric all-solid-state supercapacitors. *Nano Energy* **35**, 138, doi:10.1016/j.nanoen.2017.02.044 (2017).
6. Zheng, S. *et al.* Transition metal (Fe, Co, Ni) based metal-organic frameworks for electrochemical energy storage, Adv. Energy Mater., 1602733, doi:10.1002/aenm.201602733 (2017).
7. Yu, J. *et al.* Nanoparticle/MOF composites: preparations and applications. *Mater. Horiz.* **4**, 557, doi:10.1039/C6MH00586A (2017).
8. Zhang, L. L. & Zhao, X. S. Carbon-based materials as supercapacitor electrodes. *Chem. Soc. Rev.* **38**, 2520, doi:10.1039/B813846J (2009).
9. Zhai, Y. *et al.* Carbon materials for chemical capacitive energy storage. *Adv. Mater.* **23**, 4828, doi:10.1002/adma.201100984 (2011).
10. Lee, S. W., Gallant, B. M., Byon, H. R., Hammond, P. T. & Shao-Horn, Y. Nanostructured carbon-based electrodes: bridging the gap between thin-film lithium-ion batteries and electrochemical capacitors. *Energy Environ. Sci.* **4**, 1972, doi:10.1039/C0EE00642D (2011).
11. Lee, S. W. *et al.* Self-standing positive electrodes of oxidized few-walled carbon nanotubes for light-weight and high-power lithium batteries. *Energy Environ. Sci.* **5**, 5437, doi:10.1039/C1EE02409D (2012).
12. Hyun, T.-S., Tuller, H. L., Youn, D.-Y., Kim, H.-G. & Kim, I.-D. Facile synthesis and electrochemical properties of RuO_2 nanofibers with ionically conducting hydrous layer. *J. Mater. Chem.* **20**, 9172, doi:10.1039/C0JM00494D (2010).
13. Wu, C. H. *et al.* Preparation of novel three-dimensional NiO/ultrathin derived graphene hybrid for supercapacitor applications. *ACS Appl. Mater. Interfaces* **6**, 1106, doi:10.1021/am404691w (2014).

14. Zheng, X. *et al.* Au-embedded ZnO/NiO hybrid with excellent electrochemical performance as advanced electrode materials for supercapacitor. *ACS Appl. Mater. Interfaces* **7**, 2480, doi:10.1021/am5073468 (2015).
15. Moosavifard, S. E., El-Kady, M. F., Rahmanifar, M. S., Kaner, R. B. & Mousavi, M. F. Designing 3D highly ordered nanoporous CuO electrodes for high-performance asymmetric supercapacitors. *ACS Appl. Mater. Interfaces* **7**, 4851, doi:10.1021/am508816t (2015).
16. Xu, X., Dong, B., Ding, S., Xiao, C. & Yu, D. Hierarchical $NiCoO_2$ nanosheets supported on amorphous carbon nanotubes for high-capacity lithium-ion batteries with a long cycle life. *J. Mater. Chem. A* **2**, 13069, doi:10.1039/c4ta02003k (2014).
17. Shinde, S. K., Dubal, D. P., Ghodake, G. S. & Fulari, V. J. Hierarchical 3D-flower-like CuO nanostructure on copper foil for supercapacitors. *RSC Adv.* **5**, 4443, doi:10.1039/C4RA11164H (2015).
18. Lan, D. *et al.* Mesoporous CoO Nanocubes/continuous 3D porous carbon skeleton of rose-based electrode for high-performance supercapacitor. *ACS Appl. Mater. Interfaces* **6**, 11839, doi:10.1021/am503378n (2014).
19. Guan, Q. *et al.* Needle-like Co_3O_4 anchored on the graphene with enhanced electrochemical performance for aqueous supercapacitors. *ACS Appl. Mater. Interfaces* **6**, 7626, doi:10.1021/am5009369 (2014).
20. Zhang, W. *et al.* Fe_2O_3-decorated millimeter-long vertically aligned carbon nanotube arrays as advanced anode materials for asymmetric supercapacitors with high energy and power densities. *J. Mater. Chem. A* **4**, 19026, doi:10.1039/C6TA07720J (2016).
21. Huang, M., Li, F., Dong, F., Zhang, Y. X. & Zhang, L. L. MnO_2-based nanostructures for high-performance supercapacitors. *J. Mater. Chem. A* **3**, 21380, doi:10.1039/C5TA05523G (2015).
22. Li, W., Wang, S., Xin, L., Wu, M. & Lou, X. Single crystal β-NiS nanorod arrays with a hollow structured Ni_3S_2 framework for supercapacitor applications. *J. Mater. Chem. A* **4**, 7700, doi:10.1039/c6ta01133k (2016).
23. Ramachandran, R., Saranya, M., Grace, A. N. & Wang, F. MnS nanocomposites based on doped graphene: simple synthesis by a wet chemical route and improved electrochemical properties as an electrode material for supercapacitors. *RSC Adv.* **7**, 2249, doi:10.1039/C6RA25457H (2017).
24. Kumbhar, V. S. *et al.* Modified chemical synthesis of MnS nanoclusters on nickel foam for high performance all solid state asymmetric supercapacitors. *RSC Adv.* **7**, 16348, doi:10.1039/C7RA00772H (2017).
25. Subramani, K., Sudhan, N., Divya, R. & Sathish, M. All solid state asymmetric supercapacitors based on cobalt hexacyanoferrate-derived CoS and activated carbon. *RSC Adv.* **7**, 6648, doi:10.1039/C6RA27331A (2017).
26. Amaresh, S., Karthikeyan, K., Jang, I.-C. & Lee, Y. S. Single step microwave mediated synthesis of the CoS_2 anode material for high rate hybrid supercapacitors. *J. Mater. Chem. A* **2**, 11099, doi:10.1039/C4TA01633E (2014).
27. Zhang, K. *et al.* Hierarchical $CuCo_2O_4$ nanowire@$NiCo_2O_4$ nanosheet core/shell arrays for high performance supercapacitors. *RSC Adv.* **5**, 69636, doi:10.1039/C5RA11007F (2015).
28. Zeng, Z. *et al.* $NiCo_2S_4$ nanoparticles//activated balsam pear pulp for asymmetric hybrid capacitors. *Cryst. Eng. Comm.* **18**, 2363, doi:10.1039/C6CE00319B (2016).
29. Zhang, K. *et al.* Nanostructured Mn based oxides for electrochemical energy storage and conversion. *Chem. Soc. Rev.* **44**, 699, doi:10.1039/c4cs00218k (2015).
30. Chen, T. *et al.* All solid state high performance asymmetric supercapacitors based on novel MnS nanocrystal and activated carbon materials. *Sci. Rep.* **6**, 23289, doi:10.1038/srep23289 (2016).
31. Hou, L. *et al.* Comparative investigation of hollow mesoporous $NiCo_2S_4$ ellipsoids with enhanced pseudo-capacitances towards high-performance asymmetric Supercapacitors. *Electrochim. Acta* **214**, 76, doi:10.1016/j.electacta.2016.08.038 (2016).
32. Yang, J. *et al.* Hierarchical porous $NiCo_2S_4$ hexagonal plates: formation via chemical conversion and application in high performance supercapacitors. *Electrochim. Acta* **144**, 16, doi:10.1016/j.electacta.2014.08.040 (2014).
33. Zhu, Y., Ji, X., Wu, Z. & Liu, Y. $NiCo_2S_4$ hollow microsphere decorated by acetylene black for high-performance asymmetric supercapacitor. *Electrochim. Acta* **186**, 562, doi:10.1016/j.electacta.2015.10.176 (2015).
34. Huang, N. *et al.* Pt-sputtering-like $NiCo_2S_4$ counter electrode for efficient dye-sensitized solar cells. *Electrochimi. Acta.* **192**, 521, doi:10.1016/j.electacta.2016.02.004 (2016).
35. Lia, Z., Wu, L., Wang, L., Gu, A. & Zhou, Q. Nickel cobalt sulfide nanosheets uniformly anchored on porous graphitic carbon nitride for supercapacitors with high cycling performance. *Electrochim. Acta* **231**, 617, doi:10.1016/j.electacta.2017.02.087 (2017).
36. Yu, D. J. *et al.* Nickel cobalt sulfide nanotube array on nickel foam as anode material for advanced lithium-ion batteries. *Electrochim. Acta* **198**, 280, doi:10.1016/j.electacta.2016.01.189 (2016).
37. Jia, R., Zhu, F., Sun, S., Zhai, T. & Xia, H. Dual support ensuring high-energy supercapacitors via high-performance NiCo2S4@Fe2O3 anode and working potential enlarged MnO_2 cathode. *J. Power Sources* **341**, 427, doi:10.1016/j.jpowsour.2016.12.014 (2017).
38. Li, R., Wan, S., Huang, Z., Lu, F. & He, T. $NiCo_2S_4$@$Co(OH)_2$ core-shell nanotube arrays *in situ* grown on Ni foam for high performances asymmetric supercapacitors. *J. Power Sources* **312**, 156, doi:10.1016/j.jpowsour.2016.02.047 (2016).
39. Zhu, Y. *et al.* Mesoporous $NiCo_2S_4$ nanoparticles as high-performance electrode materials for supercapacitors. *J. Power Sources* **273**, 584, doi:10.1016/j.jpowsour.2014.09.144 (2015).
40. Su, A.-L., Lu, M.-N., Chang, C.-Y., Wei, T.-C. & Lin, J.-Y. Scalable fabrication of efficient $NiCo_2S_4$ counter electrodes for dye-sensitized solar cells using a facile solution approach. *Electrochim. Acta* **222**, 1410, doi:10.1016/j.electacta.2016.11.118 (2016).
41. Shinde, S. K. *et al.* Improved synthesis of copper oxide nanosheets and its application in development of supercapacitor and antimicrobial agents. *J. Ind. Eng. Chem.* **36**, 116, doi:10.1016/j.jiec.2016.01.038 (2016).
42. Hu, W. *et al.* $CoNi_2S_4$ nanosheet arrays supported on nickel foams with ultrahigh capacitance for aqueous asymmetric supercapacitor applications. *ACS Appl. Mater. Interfaces* **6**, 19318, doi:10.1021/am5053784 (2014).
43. Li, X., Li, Q., Wu, Y., Rui, M. & Zeng, H. Two dimensional, porous nickel–cobalt sulfide for high performance asymmetric supercapacitors. *ACS Appl. Mater. Interfaces* **7**, 19316, doi:10.1021/acsami.5b05400 (2015).
44. Wan, H. *et al.* Hierarchical configuration of $NiCo_2S_4$ nanotube@Ni–Mn layered double hydroxide arrays/three-dimensional graphene sponge as electrode materials for high-capacitance supercapacitors. *ACS Appl. Mater. Interfaces* **7**, 15840, doi:10.1021/acsami.5b03042 (2015).
45. Wei, W. *et al.* Partial ion-exchange of nickel sulfide-derived electrodes for high performance supercapacitors. *Chem. Mater.* **26**, 3418, doi:10.1021/cm5006482 (2014).
46. Zhang, Z., Wang, Q., Zhao, C., Min, S. & Qian, X. One step hydrothermal synthesis of 3D petal like Co_9S_8/RGO/Ni_3S_2 composite on nickel foam for high-performance supercapacitors. *ACS Appl. Mater. Interfaces* **7**, 4861, doi:10.1021/am5088192 (2015).
47. Zhang, G. Q. & Lou, X. W. general solution growth of mesoporous $NiCo_2O_4$ nanosheets on various conductive substrates as high-performance electrodes for supercapacitors. *Adv. Mater.* **25**, 976, doi:10.1002/adma.201204128 (2013).
48. Pu, J. *et al.* Preparation and electrochemical characterization of hollow hexagonal $NiCo_2S_4$ nanoplates as pseudocapacitor materials. *ACS Sustainable Chem. Eng.* **2**, 809, doi:10.1021/sc400472z (2014).
49. Bai, D., Wang, F., Lv, J., Zhang, F. & Xu, S. Triple confined well dispersed biactive $NiCo_2S_4$/$Ni_{0.96}S$ on graphene aerogel for high-efficiency lithium storage. *ACS Appl. Mater. Interfaces* **8**, 32853, doi:10.1021/acsami.6b11389 (2016).
50. Qian, X., Li, H., Shao, L., Jiang, X. & Hou, L. Morphology tuned synthesis of nickel cobalt selenides as highly efficient Pt-free counter electrode catalysts for dye-sensitized solar cells. *ACS Appl. Mater. Interfaces* **8**, 29486, doi:10.1021/acsami.6b09966 (2016).
51. Zhang, X. *et al.* Synthesis of porous NiO nanocrystals with controllable surface area and their application as supercapacitor electrodes. *Nano Res.* **3**(9), 643, doi:10.1007/s12274-010-0024-6 (2010).
52. Xiao, J., Wan, L., Yang, S., Xiao, F. & Wang, S. Design hierarchical electrodes with highly conductive $NiCo_2S_4$ nanotube arrays grown on carbon fiber paper for high-performance pseudocapacitors. *Nano Lett.* **14**, 831, doi:10.1021/nl404199v (2014).

53. Zhao, J., Li, Z., Zhang, M., Meng, A. & Li, Q. Vertically cross-linked and porous $CoNi_2S_4$ nanosheets-decorated SiC nanowires with exceptional capacitive performance as a free-standing electrode for asymmetric Supercapacitors. *J. Power Sources* **332**, 355, doi:10.1016/j.jpowsour.2016.09.128 (2016).
54. Li, J., Wei, M., Chu, W. & Wang, N. High-stable a-phase NiCo double hydroxide microspheres via microwave synthesis for supercapacitor electrode materials. *Chem. Eng. J.* **316**, 277, doi:10.1016/j.cej.2017.01.057 (2017).
55. Jinlong, L., Tongxiang, L., Meng, Y., Ken, S. & Hideo, M. Performance comparison of $NiCo_2O_4$ and $NiCo_2S_4$ formed on Ni foam for supercapacitor. *Composites Part B* **123**, 28, doi:10.1016/j.compositesb.2017.05.021 (2017).
56. Wan, H. Z. *et al.* $NiCo_2S_4$ porous nanotubes synthesis via sacrificial templates: high-performance electrode materials of supercapacitors. *Cryst. Eng. Comm.* **51**, 7649, doi:10.1039/C3CE41243A (2013).
57. Bonso, J. S. *et al.* Exfoliated graphite nanoplatelets-V_2O_5 nanotube composite electrodes for supercapacitors. *J. Power Sources* **203**, 227, doi:10.1016/j.jpowsour.2011.09.084 (2012).

Acknowledgements

The work is financially supported by NRF South Korea, (2017R1C1B5017360).

Author Contributions

S.K.S. and D.Y.K. synthesized the experimental part. N.M. and V.J.F. performed the experiments and electrochemical characterizations. A.A.K. and D.S.L. provided characterizations and helped for the interpretation of results. G.S.G. reviewed the data and S.K.S. wrote the manuscript. To the preparation and reviewing manuscript, all authors contributed equally.

Additional Information

Supplementary information accompanies this paper at doi:10.1038/s41598-017-10218-z

Competing Interests: The authors declare that they have no competing interests.